Supporting Information

Napetschnig *et al.* 10.1073/pnas.0813267106

SI Text

Protein Expression and Purification. DNA fragments of the Nup214 NTD and the Nup214 NTD 1–405, encompassing residues 1 to 450 and 1 to 405, respectively, were amplified by PCR from a human Nup214 cDNA construct (KIAA0023) and cloned in a pET28a vector (pET28a-PreS) modified to contain a PreScission protease-cleavable N-terminal hexa-histidine tag (1). For Nup214 NTD Δ6D7A, residues 343 to 361 were replaced by a flexible linker with the sequence GGSGG and cloned in the pET28a-PreS vector, as described above. A DNA fragment encompassing residues 343 to 361 of the Nup214 NTD 6D7A loop and followed by a hexa-histidine tag was cloned into the pGEX-6P1 vector (GE Healthcare). DNA fragments of the full-length human Ddx19, and a Dxd19 fragment, encompassing residues 1 to 300 (Ddx19 NTD), were amplified from HeLa cell cDNA, and cloned in the pET28a-PreS vector. Mutants of the Nup214 NTD and Ddx19 were generated using Quikchange site-directed mutagenesis (Stratagene). The details of the expression constructs and the mutants of Nup214 and Ddx19 are listed in Tables S2–S4.

The different constructs of Nup214 and the GST-6D7A-HIS loop fusion protein were expressed and purified as described for the Nup214 NTD (2). For expression of Ddx19, Ddx19 NTD, and Ddx19 mutants, *E. coli* BL21(DE3) cells (Stratagene) were grown at 37°C to an OD_{600} of 0.6 and induced with 450 μM isopropyl-β-D-thio-galactoside at 17°C for 9 h. Cells were harvested by centrifugation and resuspended in a lysis buffer containing 20 mM Tris, pH 8.0, 500 mM NaCl, 5 mM β-mercaptoethanol, 1 mM PMSF, and Complete EDTA-free protease inhibitor mixture tablets (Roche). The cells were lysed with a cell disrupter (Avestin), and the lysate was clarified by centrifugation at 40,000 g for 90 min. The lysate was then loaded onto a Ni-NTA column (Qiagen) and eluted via an imidazole gradient. Fractions containing hexa-histidine tagged Ddx19 were pooled, and glycerol was added to a final concentration of 10% (vol/vol). The protein was further purified after cleavage of the hexa-histidine tag with PreScission protease (GE Healthcare) by size exclusion chromatography on a 16/60 Superdex 200 column (GE Healthcare) that was equilibrated in a buffer containing 20 mM Tris, pH 8.0, 100 mM KCl, 10% glycerol, and 5 mM DTT.

For complex formation, Nup214 NTD was incubated with an equimolar amount of either Ddx19 or Ddx19 NTD and purified by size exclusion chromatography on a 16/60 Superdex 200 column (GE Healthcare) that was equilibrated in a buffer containing 20 mM Tris pH 8.0, 100 mM KCl, 5% glycerol, 5 mM DTT and 0.5 mM Mg·ADP (Spectrum Chemical). The fractions containing the complex were pooled and concentrated to 40 mg/mL for crystallization.

Protein Interaction Analysis. Protein interaction experiments were carried out on a Superdex 200 10/300 GL gel filtration column (GE Healthcare) that was equilibrated in a buffer containing 20 mM Tris, pH 8.0, 100 mM KCl, 10% (vol/vol) glycerol, and 5 mM DTT. Complexes were formed by incubating 1 mg of the various purified proteins, their mutants, or variants for 30 min at 4°C. Complex formation was monitored by injection of the preincubated proteins and the recombinant purified proteins in isolation. All proteins were analyzed under the same buffer conditions, and complex formation was confirmed by SDS/PAGE of the eluted fractions followed by Coomassie brilliant blue staining.

Peptide Binding Assay. A peptide array composed of 20-mers with an offset of 3 residues covering the entire sequence of human Ddx19 was synthesized and immobilized onto a nitrocellulose membrane (Rockefeller University Proteomics Resource Center). The peptide array was blocked for 7 h in TBS-Tween buffer supplemented with 5% (wt/vol) milk powder and washed 3 times for 10 min in TBS-Tween buffer followed by a single wash step in transport buffer (20 mM Hepes-KOH, pH 7.5, 110 mM potassium acetate, 2 mM $MgCl_2$, 0.1% Tween-20). The peptide array was then incubated with the in vitro transcribed, translated, and [35S]-methionine-labeled Nup214 NTD (Promega, TnT quick coupled Transcription/Translation system) in transport buffer at 4°C. Before detection by autoradiography, the membrane was washed 4 times for 10 min with transport buffer.

Generation of a Ddx19 Homology Model. Based on the structure of the *M. jannaschii* DEAD-box helicase MjDEAD (PDB code 1HV8) (3) and a sequence alignment of 10 eukaryotic Ddx19 homologs (Fig. S1), we generated a homology model for human Ddx19 using MODELLER (4). Although the central core region that contains the 10 conserved sequence motifs aligned without major sequence gaps, the Ddx19-specific N-terminal sequence is not conserved in MjDEAD. Hence, we were able to generate a model for the core region, but we are unable to model the unique N-terminal extension of Ddx19.

Crystallization and Data Collection. Crystals of human Nup214 NTD•Ddx19 and Nup214 NTD•Ddx19 NTD were grown at 21°C in hanging drops containing 1 μL of the protein (40 mg/mL), which contained 0.5 mM Mg•ADP and 1 μL of a reservoir solution. Crystals of Nup214 NTD•Ddx19 and Nup214 NTD•Ddx19 NTD grew in 0.1 M CHES, pH 9.5, 30% PEG 3000, and in 0.1 M sodium acetate, pH 4.2–4.5, 0.8 M sodium di-hydrogen phosphate, and 1.2 M di-potassium hydrogen phosphate, respectively. For cryoprotection, Nup214 NTD•Ddx19 and Nup214 NTD•Ddx19 NTD crystals were stabilized and cryo-protected in 0.1 M CHES, pH 9.5, 30% (vol/vol) PEG 3000, supplemented with 10% (vol/vol) glycerol, and in 0.1 M sodium acetate, pH 4.2, 0.8 M sodium di-hydrogen phosphate, 1.2 M di-potassium phosphate, supplemented with 20% (vol/vol) glycerol, respectively, and flash frozen in liquid nitrogen-cooled liquid propane. X-ray diffraction data were collected at beamlines 8.2.1 and 8.2.2 at the Advanced Light Source, Lawrence Berkeley National Laboratory. X-ray intensities were processed and integrated using the HKL2000 denzo/scalepack package (5), and the CCP4 program package was used for subsequent calculations (6).

Structure Determination. The structure of the Nup214 NTD•Ddx19 was solved by molecular replacement, using the coordinates of the Nup214 NTD (2) as a search model in PHASER (7). This resulting electron density map was of high quality and clearly revealed additional density for the N-terminal domain of Ddx19. A model was built with the program O (8) and refined with CNS (9). No electron density was observed for the N-terminal 8 and C-terminal 22 residues of Nup214, and the N-terminal 69 and C-terminal 181 residues that encompass the entire C-terminal RecA-like domain (domain 2) of Ddx19. These residues are presumed to be disordered, and, therefore, have been omitted from the final model. The final model contains residues 9 to 428 and 70 to 298 of Nup214 and Ddx19,

respectively, and has been refined to 3.2 Å resolution with an R_{cryst} factor of 24.9% and an R_{free} factor of 28.3%.

The structure of the Nup214 NTD•Ddx19 NTD complex was determined using the coordinates of the refined Nup214 NTD•Ddx19 complex as a search model in PHASER (7). The final rounds of refinement were carried out with REFMAC, using the TLS option (10). The final model contains residues 8 to 428 and 69 to 300 of Nup214 and Ddx19, respectively, and has been refined to 2.5 Å resolution with an R_{cryst} factor of 19.9% and an R_{free} factor of 24.2%. The stereochemical quality of the final models was assessed with PROCHECK (11) and Molprobity (12). Met-291 in Nup214 is the only outlier in the Nup214 NTD•Ddx19 NTD structure. However, this residue is well defined in the electron density map and is located in a canonical β-turn type II' (13). Data collection and refinement statistics are shown in the Table S1.

Immunofluorescence Confocal Microscopy. For immunofluorescence, Ddx19, Nup214 NTD, and their mutants and variants were cloned into the pCMV-HA vector (Clontech) containing a C-terminal HA-tag. The details of the Nup214 and Ddx19 constructs are listed in Table S4. Mammalian cell culture and transfection of HeLa cells were performed as described in ref. 14. HeLa cells were washed in PBS and fixed for 20 min in 4% PFA (Wako) at room temperature (RT) and then washed twice with PBS again. Cells were then permeabilized with 0.3% Digitonin (Electron Microscope Sciences) and 1% BSA (Sigma) in PBS for 10 min at RT. Cells were blocked with 3% BSA in PBS for 20 min.

For Ddx19 variants, the cells were incubated with α-HA (at a dilution of 1:2,000, Abcam) for 1 h at RT. The cells were washed twice with PBS and were incubated with secondary antibody (goat α-rabbit Alexa Fluor 488, at a dilution of 1:2,000, Invitrogen) for 1 h at RT. The cells were further incubated with α-mAb414 (at a dilution 1:1,000, Covance) for 1 h at RT, washed twice with PBS, incubated with secondary antibodies (goat α-mouse Rodamine-Red X, at a dilution of 1:1,000, Invitrogen) for 1 h at RT and mounted onto cover slips with ProLong Gold Antifade reagent (Invitrogen). Samples were examined on a Zeiss LSM5 EXCITER confocal microscope, and all images acquired by using an aplan-Apochromat 63X with an 1.4-n.a. objective.

For Nup214 variants, the cells were costained with a mouse α-HA antibody (at a dilution of 1:1,000, Covance) and a rabbit α-Nup358 antibody (at a dilution of 1:500) (15) for 1 h at RT. The cells were washed 3 times with PBS, incubated with secondary antibodies for 1 h at RT (goat α-rabbit Alexa Fluor 488, goat α-rabbit Alexa Fluor 647; both at a dilution of 1:200, Molecular Probes), washed 3 times with PBS, and mounted in Fluoromount G (Electron Microscopy Sciences). The samples were examined using a Leica spectral confocal microscope (model TCS SP).

Illustrations and Figures. Figures were generated using PyMOL (www.pymol.org). The molecular surfaces were calculated using MSMS (16), and the electrostatic potential was calculated using APBS (17). Sequence alignments were generated using ClustalX (18) and colored with Alscript (19).

1. Hoelz A, Nairn AC, Kuriyan J (2003) Crystal structure of a tetradecameric assembly of the association domain of Ca^{2+}/calmodulin-dependent kinase II. *Mol Cell* 11:1241–1251.
2. Napetschnig J, Blobel G, Hoelz A (2007) Crystal structure of the N-terminal domain of the human protooncogene Nup214/CAN. *Proc Natl Acad Sci USA* 104(6):1783–1788.
3. Story RM, Li H, Abelson JN (2001) Crystal structure of a DEAD box protein from the hyperthermophile Methanococcus jannaschii. *Proc Natl Acad Sci USA* 98(4):1465–1470.
4. Eswar N, Webb B, Marti-Renom MA, Madhusudhan MS, Eramian D, Shen MY, Pieper U, Sali A (2006) Comparative protein structure modeling using Modeller. Curr Protoc Bioinformatics Chapter 5, Unit 5 6 (2006). *Curr Protoc Bioinformatics* Chapter 5, Unit 5 6.
5. Otwinowski Z, Minor W (1997) Processing of X-Ray diffraction data collected in oscillation mode. *Methods Enzymol* 276:307–326.
6. (1994) The CCP4 suite: Programs for protein crystallography. *Acta Crystallogr D Biol Crystallogr* 50:760–763.
7. McCoy AJ (2007) Solving structures of protein complexes by molecular replacement with Phaser. *Acta Crystallogr D Biol Crystallogr* 63(Pt 1):32–41.
8. Jones TA, Zou JY, Cowan SW, Kjeldgaard M (1991) Improved methods for building protein models in electron density maps and the location of errors in these models *Acta Crystallogr A* 47(Pt 2):110–119.
9. Brunger AT, et al. (1998) Crystallography and NMR system: A new software suite for macromolecular structure determination. *Acta Crystallogr D* 54(Pt 5):905–921.
10. Murshudov GN, Vagin AA, Dodson EJ (1997) Refinement of macromolecular structures by the maximum-likehood method. *Acta Crystallogr D* 53(Pt 3):240–255.
11. Laskowski RA, MacArthur MW, Moss DS, Thornton, JM (1993) PROCHECK: A program to check the stereochemical quality of protein structures. *J Appl Crystallogr* 26:283–291.
12. Davis IW, Leaver-Fay A, Chen VB, Block JN, Kapral GJ, Wang X, Murray LW, Arendall WB, 3rd, Snoeyink J, Richardson JS, Richardson DC (2007) MolProbity: All-atom contacts and structure validation for proteins and nucleic acids. *Nucleic Acids Res* 35:W375–83.
13. Richardson JS (1981) The anatomy and taxonomy of protein structure. *Adv Protein Chem* 34:167–339.
14. Wong RW, Blobel G, Coutavas E (2006) Rae1 interaction with NuMA is required for bipolar spindle formation. *Proc Natl Acad Sci USA* 103:19783–7.
15. Wu J, Matunis MJ, Kraemer D, Blobel G, Coutavas E (1995) Nup358, a cytoplasmically exposed nucleoporin with peptide repeats, Ran-GTP binding sites, zinc fingers, a cyclophilin A homologous domain, and a leucine-rich region. *J Biol Chem* 270:14209–13.
16. Sanner MF, Spehner JC, Olson AJ (1996) Reduced surface: An efficient way to compute molecular surfaces. *Biopolymers* 38(3):305–320.
17. Baker NA, Sept D, Joseph S, Holst MJ, McCammon JA (2001) Electrostatics of nanosystems: Application to microtubules and the ribosome. *Proc Natl Acad Sci USA* 98:10037–41.
18. Jeanmougin F, Thompson JD, Gouy M, Higgins DG, Gibson TJ (1998) Multiple sequence alignment with Clustal X. *Trends Biochem Sci* 23:403–405.
19. Barton GJ (1993) ALSCRIPT: A tool to format multiple sequence alignments. *Protein Eng* 6:37–40.

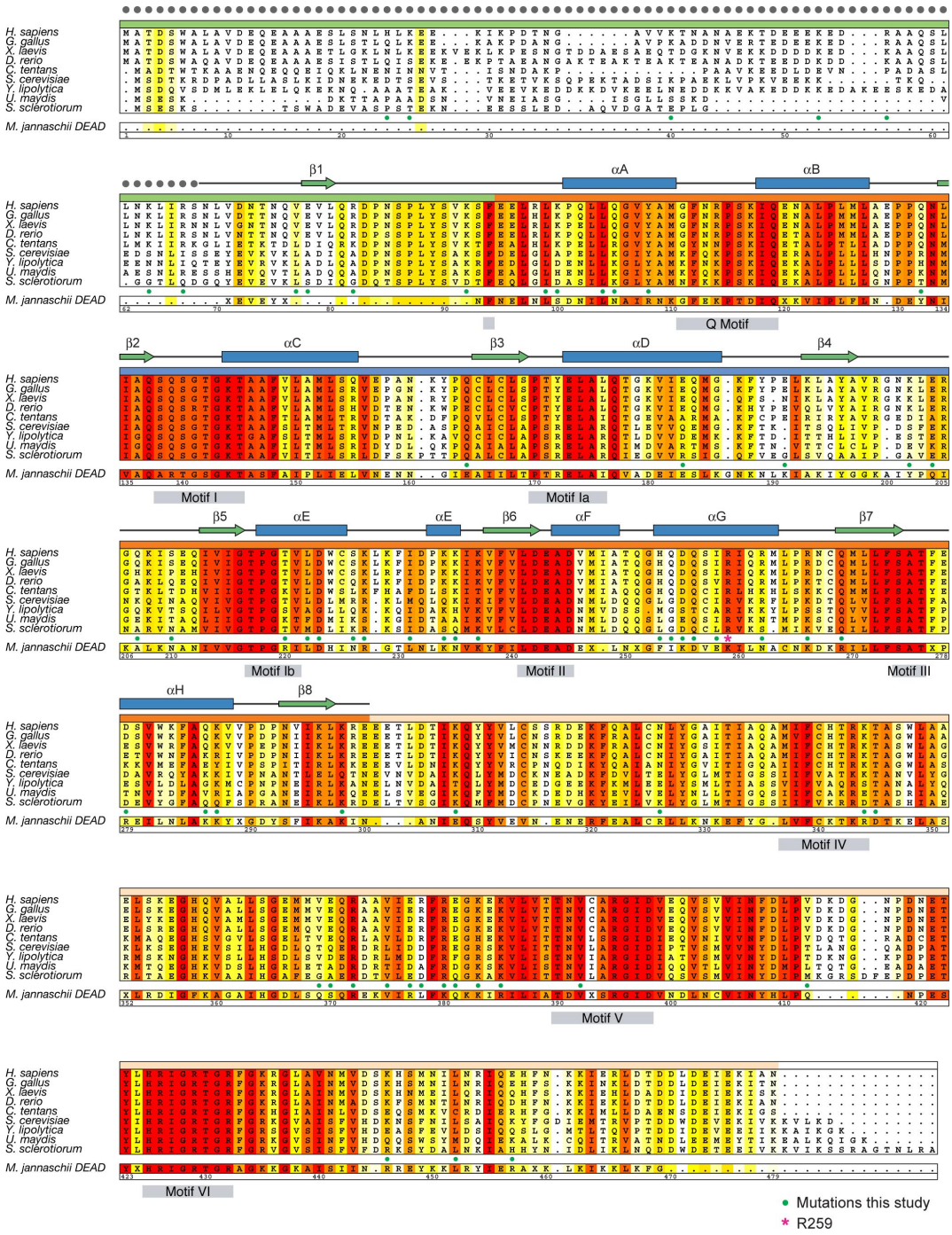

Fig. S1. Multispecies sequence alignment of Ddx19 homologs. The overall sequence conservation at each position is shaded in a color gradient from yellow (60% similarity) to dark red (100% identity), using the Blosum62 weighting algorithm. The secondary structure of Ddx19 as observed in the Nup214 NTD•Ddx19 structure is shown above the alignment. The residue numbering is relative to *H. sapiens* Ddx19 and gray boxes below the alignment indicate the position of the 9 conserved DEAD-box helicase motifs. As a reference, the primary sequence of the *M. janaschii* DEAD-box protein MjDEAD is aligned with the Ddx19 homologs.

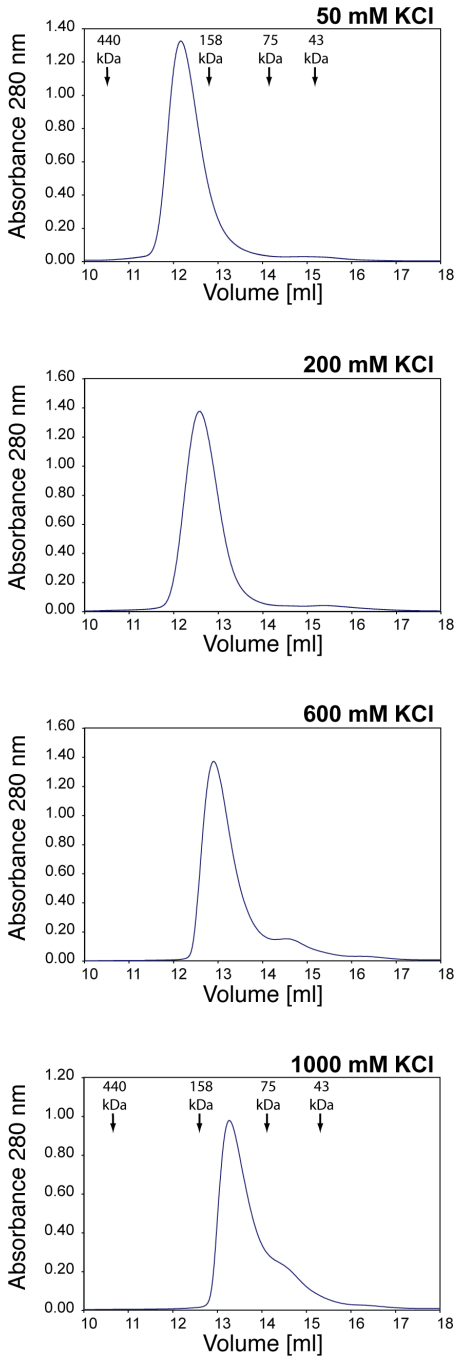

Fig. S2. Salt dependence of the Nup214–Ddx19 interaction. Gel filtration profiles of the Nup214•Ddx19 complex at identical protein complex concentrations of 50 μM and the indicated salt concentrations. The elution positions for molecular weight standards are indicated.

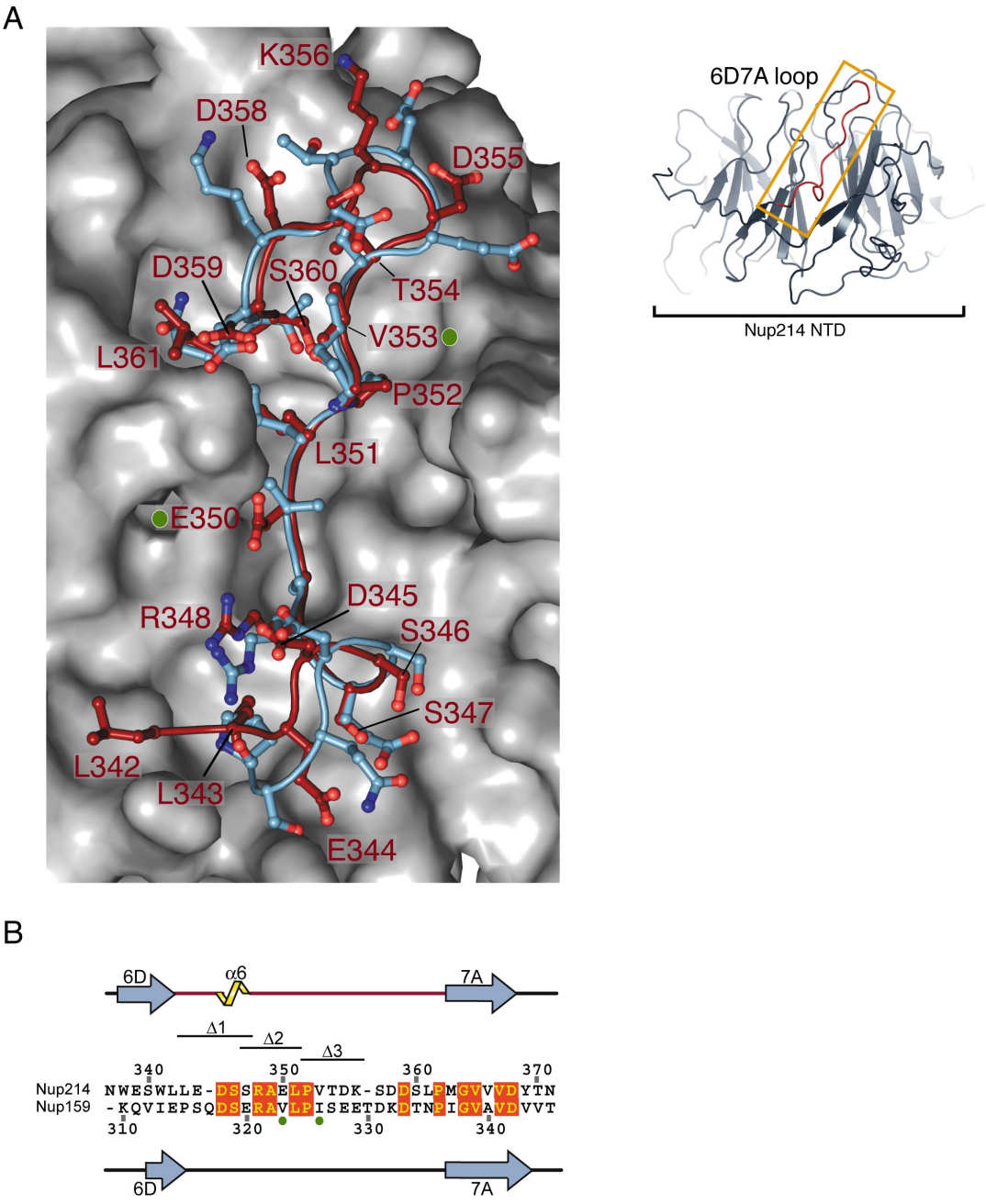

Fig. S3. Comparison of the 6D7A loops of the human Nup214 and the yeast Nup159 β-propeller domains. (*A*) Structural alignment of the 6D7A loops of the homologous human and yeast β-propellers. The surface of the Nup214 β-propeller domain omitting the 6D7A loop is shown in a gray surface rendition. The Cα-traces of the 6D7A loop of Nup214 (red) and Nup159 (blue) are shown in coil representation and side chains in ball-and-stick representation. For clarity, only the Nup214 residues are numbered. The localizations of the Nup159 mutants V323E and I326E that abolish complex formation with the yeast Dbp5 helicase are indicated by green dots. (*B*) Structure-based sequence alignment of the Nup214 and Nup159 6D7A loops. The secondary structure and residue numbering are indicated above and below the sequence for Nup214 and Nup159, respectively. The localization of the Nup159 double mutant V323E/I326E is labeled by green dots, and conserved residues are highlighted. The residues of the 6D7A loop that are deleted in the Nup214 NTD Δ1, Δ2, and Δ3 variants are indicated.

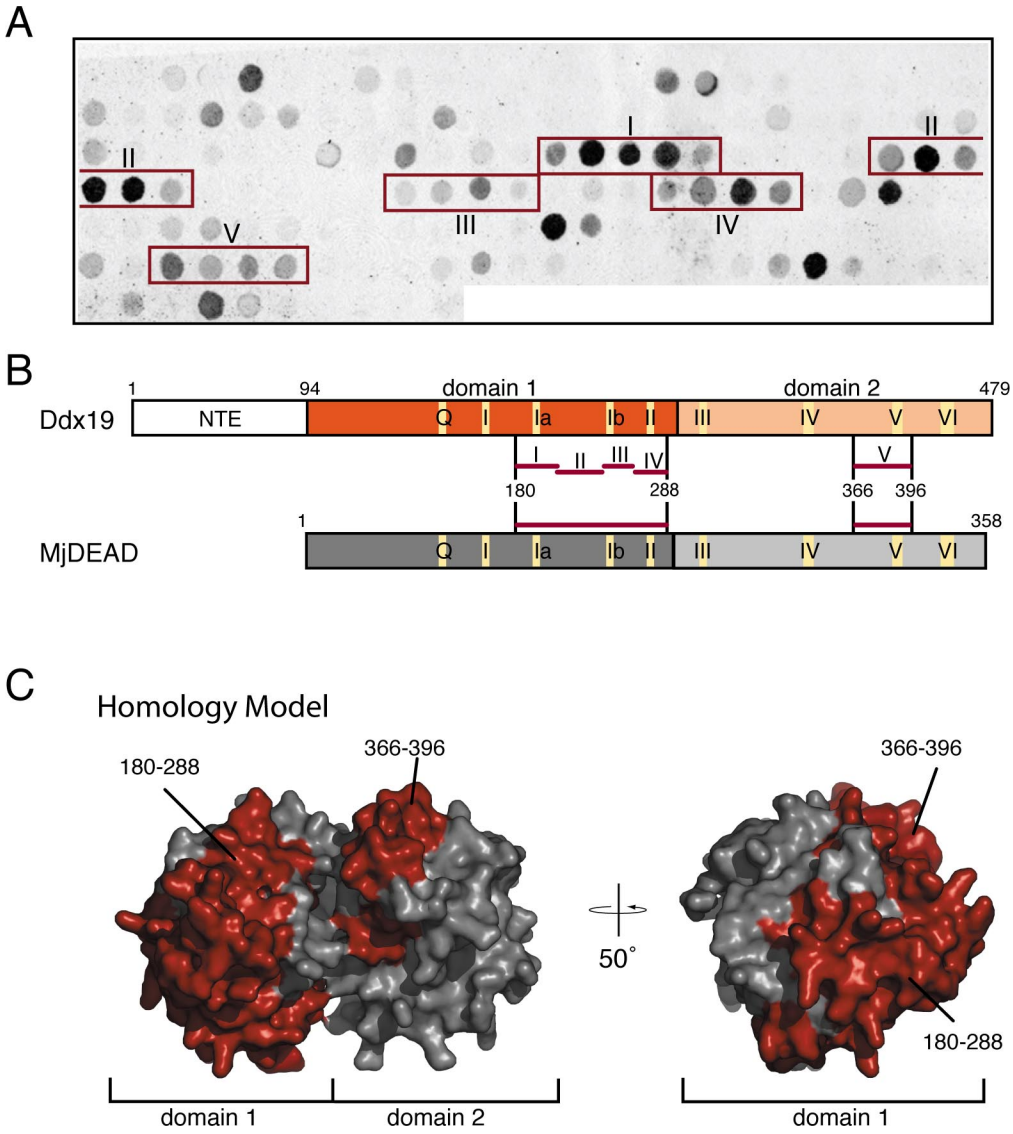

Fig. S4. Analysis of the Nup214•Ddx19 interaction by peptide array. (*A*) Ddx19 peptide array probed with the radioactively labeled Nup214 NTD. The 5 identified regions containing at least 4 consecutive peptide spots are numbered I to V and are indicated by a red box. (*B*) Domain structures of Ddx19 and the *M. jannaschii* DEAD-box protein MjDEAD, displaying the 9 conserved sequence motifs as indicated in Fig. S1. The 5 identified regions and their corresponding residues are indicated. (*C*) Homology model of Ddx19 in surface representation based on MjDEAD (PDB code 1HV8) (3). Identified peptides were mapped onto the surface and colored in red. The residue numbering is relative to human Ddx19.

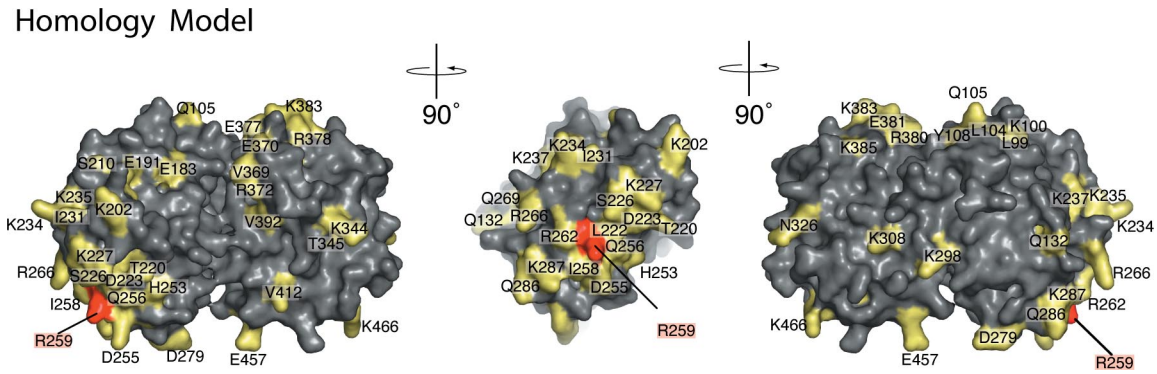

Fig. S5. Alanine-scanning mutagenesis of Ddx19. Homology model of Ddx19 illustrating the approximate location of mutated Ddx19 surface residues. Alanine mutants that were capable of interacting with Nup214 are shown in yellow, and mutant R259A, which is incapable of interacting with Nup214, is shown in red. The residue numbering is relative to human Ddx19.

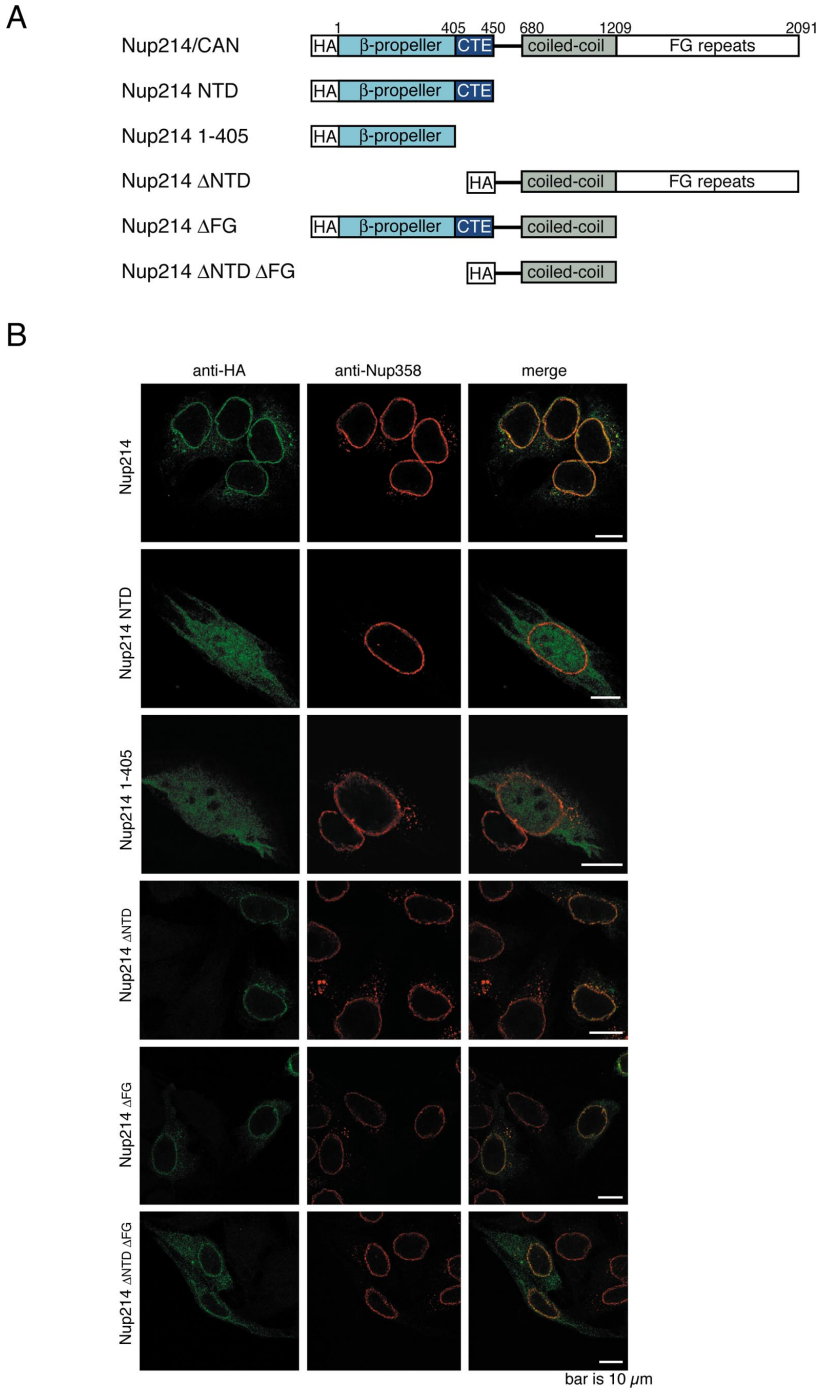

Fig. S6. In vivo localization of Nup214 and Nup214 fragments. (*A*) The domain organization of Nup214 and the various Nup214 fragments are indicated. (*B*) HeLa cells were transfected with Nup214 and Nup214 fragments containing a C-terminal HA-tag and analyzed with confocal microscopy. The cellular localization of the HA-tagged Nup214 proteins was detected with an α-HA antibody (green). The polyclonal α-Nup358 antibody was used as a reference for nuclear envelope staining (red). The merged image is shown on the right.

Table S1. Crystallographic analysis

	Crystal 1 native	Crystal 2 native
Contents		
Nup214	Nup214 NTD	Nup214 NTD
Ddx19	Ddx19, residues 1–300	Ddx19, residues 1–479
Data collection		
Synchrotron	ALS	ALS
Beamline	BL8.2.2	BL8.2.1
Space group	$P2_12_12_1$	$P2_1$
Cell dimensions, Å		
a	59.5	61.4
b	115.4	112.9
c	143.5	142.6
Cell dimensions, °		
α	90	90
β	90	89.9
γ	90	90
Wavelength, Å	1.0000	0.9795
Resolution, Å	50.0–2.5	50.0–3.2
R_{sym},* %	10.5 (68.7)	11.3 (39.5)
$\langle I/\sigma I \rangle$*	25.0 (2.7)	14.3 (3.6)
Completeness,* %	98.6 (89.9)	91.3 (70.9)
Redundancy*	13.8 (10.8)	6.8 (5.9)
Refinement		
Resolution, Å	50.0–2.5	50.0–3.2
No. reflections		
Total	29,350	28,125
Test set, %	1,528 (4.9)	1,504 (5.1)
R_{work}/R_{free}, %	19.9/24.2	24.9/28.3
No. atoms	5,183	10,218
Protein	5,118	10,164
Ligand/ion	33	54
Water	32	0
B factors	59	86
Protein	58	86
Ligand/ion	60	89
Water	49	N.A.
rmsd		
Bond lengths, Å	0.014	0.013
Bond angles, °	1.5	1.5
Ramachandran statistics		
Most favored, %	89.7	82.1
Additionally allowed, %	9.4	16.5
Generously allowed, %	0.7	1.3
Disallowed, %	0.2	0.0

*Highest-resolution shells are shown in parentheses.

Table S2. Nup214 NTD mutants

Deletions	Alanine mutants
Nup214 NTD	Nup214 NTD L343A
Nup214 NTD 1–405	Nup214 NTD D345A
Nup214 NTD Δ6D7A	Nup214 NTD S346A
Nup214 NTD Δ1	Nup214 NTD R348A
Nup214 NTD Δ2	Nup214 NTD E350A
Nup214 NTD Δ3	Nup214 NTD V353A
GST-6D7A-His_6	Nup214 NTD T354A
	Nup214 NTD D355A
	Nup214 NTD K356A
	Nup214 NTD S357A
	Nup214 NTD D358A
	Nup214 NTD D359A
	Nup214 NTD V353E
	Nup214 NTD E350A/V353E

Table S3. Ddx19 mutants

NTE mutants	Domain 1 mutants	Domain 2 mutants
H24A	L99A	R262A
K26A	K100A	R266A
K40A	L104A*	Q269A
K53A	Q105A	D279A*
R56A	Y108A	Q286A
K64A	Q132A	K287A
R67A	Q164A	K298A
V77A	E183A	K308A
E78A	E191A	N326A
R82A	K202A	K344A
K92A	E204A	T345A
	Q207A	V369A
	S210A	E370A
	T220A	R372A
	L222A	V375A*
	D223A	E377A*
	S226A	R378A
	K227A	R380A
	I231A	E381A
	K234A	K383A
	K235A	K385A
	K237A*	V392A
	H253A	V412A
	Q254A	K446A
	D255A	L452A*
	Q256A	E457A
	I258A	
	R259A	
	R259E	
	R259Q	
	R259K	

*Proteins degraded during purification.

Table S4. Protein expression and immunofluorescence microscopy constructs

Protein	Residues	Vector	Restriction sites 5′, 3′	Tags N/C
Expression constructs				
Nup214 NTD	1–450	pET28a-PreS	NdeI, NotI	His_6/none
Nup214 mutants	1–450	pET28a-PreS	NdeI, NotI	His_6/none
Nup214 NTD 1–405	1–405	pET28a-PreS	NdeI, NotI	His_6/none
Nup214 NTD Δ6D7A	1–342,GGSGG, 362–450	pET28a-PreS	NdeI, NotI	His_6/none
Nup214 NTD Δ1	1–342, 348–450	pET28a-PreS	NdeI, NotI	His_6/none
Nup214 NTD Δ2	1–347, 352–450	pET28a-PreS	NdeI, NotI	His_6/none
Nup214 NTD Δ3	1–352, 357–450	pET28a-PreS	NdeI, NotI	His_6/none
GST-6D7A-His_6	343–361	pGEX-6P1	EcoRI, NotI	GST/His_6
Ddx19 Full-length	1–479	pET28a-PreS	NdeI, NotI	His_6/none
Ddx19 NTD	1–300	pET28a-PreS	NdeI, NotI	His_6/none
Ddx19 mutants	1–479	pET28a-PreS	NdeI, NotI	His_6/none
Immunofluorescence microscopy constructs				
Nup214	1–2091	pCMV	EcoRI, NotI	HA
Nup214 NTD	1–450	pCMV	EcoRI, NotI	HA
Nup214 NTD1–405	1–405	pCMV	EcoRI, NotI	HA
Nup214 ΔNTD	451–2091	pCMV	EcoRI, NotI	HA
Nup214 ΔFG	1–1209	pCMV	EcoRI, NotI	HA
Nup214 ΔNTDΔFG	451–1209	pCMV	EcoRI, NotI	HA
Ddx19 Full-length	1–479	pCMV	EcoRI, NotI	HA
Ddx19 R259A	1–479	pCMV	EcoRI, NotI	HA
Ddx19 R259K	1–479	pCMV	EcoRI, NotI	HA